

## A MAGNETIC RIBBON MODEL FOR STAR-FORMING FILAMENTS

SAYANTAN AUDDY<sup>1</sup>, SHANTANU BASU<sup>1</sup>, AND TAKAHIRO KUDOH<sup>2</sup>*Draft version September 13, 2016*

## ABSTRACT

We develop a magnetic ribbon model for molecular cloud filaments. These result from turbulent compression in a molecular cloud in which the background magnetic field sets a preferred direction. We argue that this is a natural model for filaments and is based on the interplay between turbulence, strong magnetic fields, and gravitationally-driven ambipolar diffusion, rather than pure gravity and thermal pressure. An analytic model for the formation of magnetic ribbons that is based on numerical simulations is used to derive a lateral width of a magnetic ribbon. This differs from the thickness along the magnetic field direction, which is essentially the Jeans scale. We use our model to calculate a synthetic observed relation between apparent width in projection versus observed column density. The relationship is relatively flat, similar to observations, and unlike the simple expectation based on a Jeans length argument.

*Subject headings:* ISM: clouds — magnetic fields — magnetohydrodynamics (MHD) — stars: formation — turbulence

## 1. INTRODUCTION

The *Herschel Space Observatory* has revealed a wide-ranging network of elongated (filamentary) structures in molecular clouds (e.g., André et al. 2010; Men'shchikov et al. 2010). Even though filamentary structures in molecular clouds were already well established (e.g., Schneider & Elmegreen 1979), the Herschel continuum maps of dust emission at 70-500  $\mu\text{m}$  have achieved unprecedented sensitivity and revealed a deeper network of filaments, in both star-forming and non-star-forming molecular clouds. This implies that the filamentary network is an imprint of initial conditions, likely turbulence, rather than the result of pure gravitational instability. Furthermore, the prestellar cores and proto-stars, when present, are preferentially found along massive filaments.

Much interpretation of the filaments has been based on the assumption that they are isothermal cylinders. This simplifies their analysis as their observed shape is then independent of most viewing angles and one can rely on established theoretical results about the equilibrium or collapse of infinite cylinders. André et al. (2010) interpreted the observations in terms of the critical line mass of an isothermal cylinder  $m_{\text{l,crit}} = 2c_s^2/G$ , where  $c_s$  is the isothermal sound speed. For a mass per unit length  $m > m_{\text{l,crit}}$ , a cylinder undergoes indefinite collapse as long as the gas is isothermal, and for  $m < m_{\text{l,crit}}$  it can settle into an equilibrium structure, although still unstable to clumping along its length into Jeans length sized fragments (Larson 1985). André et al. (2010) argue that star formation is initiated when  $m > m_{\text{l,crit}}$ .

A challenge to the view of filaments as cylinders is the magnetic field alignment inferred from polarized emission. Palmeirim et al. (2013) find that large scale magnetic fields are aligned perpendicular to the

long axis of the massive star-forming filaments (see also Planck Collaboration et al. 2016). This makes a circular symmetry of a cylinder about the long axis unlikely unless the magnetic field strength is dynamically insignificant. A more natural configuration is a magnetic ribbon, a triaxial object that is flattened along the direction of the large-scale magnetic field with its shortest dimension in that direction. In the lateral direction to the magnetic field, elongated structures can form due to turbulence and gravity. Indeed, simulations of turbulence accelerated star formation in a strongly magnetic medium (Li & Nakamura 2004; Nakamura & Li 2005; Kudoh & Basu 2008; Basu et al. 2009; Kudoh & Basu 2011) show the formation of ribbon-like structure in a layer that is flattened along the magnetic field direction. Magnetic ribbons have recently been investigated theoretically by Tomisaka (2014) and Hanawa & Tomisaka (2015). They study magnetohydrostatic equilibria of ribbons that arise from a parent filament of radius  $R_0$ , which is a free parameter in the problem. They find that a critical line-mass-to-flux ratio exists for collapse, in analogy to the critical mass-to-flux ratio for axisymmetric three-dimensional objects (Mouschovias & Spitzer 1976).

A further challenge to filaments modeled as isothermal cylinders comes from the dust emission measurement of the FWHM of the mean column density profile relative to the axis of a filament (Arzoumanian et al. 2011). For example, figure 7 of Arzoumanian et al. (2011) shows that the FWHM values for 90 filamentary structures in low mass star forming regions cluster around a mean of  $\sim 0.1$  pc with some scatter over two orders of magnitude range of mean column density<sup>3</sup>. However, Ostriker (1964) showed that the central half-mass radius of an equilibrium isothermal cylinder is  $a \propto c_s/\sqrt{G\rho_c}$ , essentially the Jeans length, where  $\rho_c$  is the central density. The projected column density of such a circularly sym-

sauddy3@uwo.ca, basu@uwo.ca

kudoh@nagasaki-u.ac.jp

<sup>1</sup> Department of Physics and Astronomy, The University of Western Ontario, London, ON N6A 3K7, Canada.<sup>2</sup> Faculty of Education, Nagasaki University, 1-14 Bunkyo-machi, Nagasaki 852-8521, Japan.<sup>3</sup> Molecular line emission studies of the Taurus region show wider mean thicknesses  $\sim 0.4$  pc for filaments in velocity-integrated emission and  $\sim 0.2$  pc for filaments in individual velocity channels (Panopoulou et al. 2014)

metric configuration has a central flat region of size  $a$  and column density  $\Sigma_c = 2\rho_c a$  (see Dapp & Basu 2009), so that we can also write  $a \propto c_s^2/(G\Sigma_c)$ . Therefore, the approximate observed relation  $a \simeq \text{constant}$  is unlike the expected  $a \propto \Sigma_c^{-1}$ . However, the observed set of values of the FWHM radii also intersect the line of Jeans length at the median log column density, which implies that the Jeans length may not be wholly unrelated to them.

In this paper, we explore the consequences of a magnetic ribbon model for molecular cloud filaments for the measured relation between apparent width and the observed column density. We argue that this is a more natural model for filaments and is based on the interplay between turbulence, strong magnetic fields, and gravitationally-driven ambipolar diffusion, rather than pure gravity and thermal pressure. We extend the analytic model of Kudoh & Basu (2014) for the formation of magnetic ribbons that is based on numerical simulations. We derive a lateral width of a magnetic ribbon and use it to calculate a synthetic observed relation between apparent width in projection versus observed column density.

## 2. SEMI-ANALYTIC MODEL

### 2.1. Background

Dynamically important magnetic fields, corresponding to mass-to-flux ratios that range from subcritical to mildly supercritical, will lead to flattening along the magnetic field direction, and subsequent evolution will be primarily perpendicular to the magnetic field (Fiedler & Mouschovias 1993; Nakamura & Li 2008). Even highly turbulent three-dimensional simulations (Kim & Basu 2013) show that the turbulence is eventually dominated by motions perpendicular to the ambient magnetic field. Observations of some filaments (e.g., Palmeirim et al. 2013) that show a large-scale magnetic field along the short dimension of the filament also support the idea of flattening along the field. In this paper, we adopt the scenario of turbulent compression acting primarily perpendicular to the magnetic field direction in an initially subcritical molecular cloud. This leads to the paradigm of turbulence accelerated star formation, in which star formation occurs with globally low efficiency and in turbulent compressed regions. These regions oscillate about an approximate force-balanced state until ambipolar diffusion creates supercritical pockets that collapse to form stars. We explore the consequences of this scenario by extending a semi-analytic model of Kudoh & Basu (2014) that is based on numerical simulations.

### 2.2. Ribbon Width

We consider local pressure balance of a compressed region in a subcritical cloud and neglect thermal pressure in comparison to magnetic pressure and the ram pressure of the flow. We assume that the cloud is stratified in the  $z$ -direction, with compression happening primarily in the  $x$ - $y$  plane. Here we simplify the analysis of the compression by limiting it to one direction, the  $x$ -axis (Fig. 2.2), as done by Kudoh & Basu (2014). The initial magnetic field strength is  $B_0$  and the field strength increases upon compression until the magnetic pressure within the compressed ribbon balances the external ram pressure and magnetic pressure. Hence the compression

ends (and oscillations may ensue) when

$$H \frac{B^2}{8\pi} = H_0 \left( \rho_0 v_{t0}^2 + \frac{B_0^2}{8\pi} \right), \quad (1)$$

where  $v_{t0}$  is the nonlinear flow speed. Assuming that the gas has adequate time to settle into hydrostatic equilibrium along the  $z$ -direction, the half thickness of the cloud is

$$H = \frac{c_s}{\sqrt{2\pi G\rho}} \quad (2)$$

(Spitzer 1942). Now if the ambipolar diffusion time is longer than the compression time (Kudoh & Basu 2014), flux freezing is valid during compression, i.e.,

$$\frac{B}{\Sigma} = \frac{B_0}{\Sigma_0}. \quad (3)$$

For the surface density  $\Sigma = 2\rho H$ , equation (3) can be rewritten as

$$\frac{B}{\rho^{\frac{1}{2}}} = \frac{B_0}{\rho_0^{\frac{1}{2}}}. \quad (4)$$

Using equation (2) and equation (4) in equation (1) and with some simplifications we get

$$\left( \frac{\rho}{\rho_0} \right)^{1/2} = 2 \left( \frac{v_{t0}}{v_{A0}} \right)^2 + 1, \quad (5)$$

where  $v_{A0}^2 = B_0^2/(4\pi\rho_0)$  is the square of the initial Alfvén speed of the cloud. The consequence of such compression results in the formation of magnetic ribbons of width  $L$  and thickness  $2H$ , as they are flattened along the direction of magnetic field (see Fig. 2.2). For conservation of mass per unit length in the ribbon during the compression of the cloud

$$\rho_0 L_0 H_0 = \rho L H, \quad (6)$$

where  $L_0$  is the initial width (along the  $x$ -axis) and  $2H_0$  is the initial thickness of the cloud in the vertical direction ( $z$ -axis). Using equation (2), we can simplify the above equation to

$$\left( \frac{\rho}{\rho_0} \right)^{1/2} = \frac{L_0}{L}. \quad (7)$$

By using equation (7) in equation (5), we can express the final width of the filament as

$$L = L_0 \left[ 2 \left( \frac{v_{t0}}{v_{A0}} \right)^2 + 1 \right]^{-1}. \quad (8)$$

Analysis of Zeeman measurements of the magnetic field in molecular clouds presented by Crutcher (1999) shows that the turbulent line width is comparable to the Alfvén speed (Basu 2000). If we make the plausible estimate that the flow speed is comparable to the Alfvén speed, i.e.,  $v_{t0} \simeq v_{A0}$ , the filament width becomes

$$L \simeq L_0/3. \quad (9)$$

The result illustrates the fact that the final width of a filament is *independent* of the density of the medium. Instead it is a fraction of the initial length scale  $L_0$  of the compressed region.

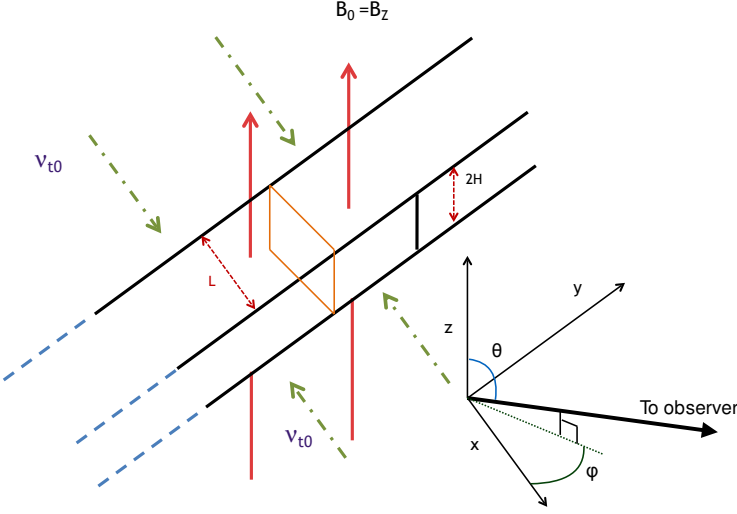


**Figure 1.** The formation of a magnetic ribbon as the molecular cloud contracts under the influence of the “ram pressure” and the perpendicular magnetic field. The thick black arrow points to an observer located at a random orientation in the sky.

### 2.3. Initial Compression Scale

In the above theory, the final ribbon width  $L$  is independent of its density, but does depend on the initial compression scale  $L_0$  associated with turbulence. The origin and physics of  $L$  is then quite different than that of the Jeans length. What is  $L_0$  then? In the turbulent scenario that we adopt in this study, it would be associated with the dominant mode in the turbulent flow field in a molecular cloud. At this point, no first principles theory exists to calculate  $L_0$  as the preferred mode of an instability that leads to molecular cloud turbulence. Hence, we take guidance from observations to make an empirical estimate for  $L_0$ .

#### 2.3.1. Estimate from column density map

The column density maps used by Arzoumanian et al. (2011) to determine the mean filament width can also be used to estimate a mean spacing between filaments, which we identify with  $L_0$  in our model. Figure 3b of Arzoumanian et al. (2011) identifies 27 filaments in a dust emission map of the cloud IC 5146. We use this same map to make an approximate measurement of  $L_0$ . For each of the 27 filaments, we identify a center along the length (spine) of the filament. Then for each filament we measure the distance to the nearest center point of another filament. We obtain a set of 20 unique distance measurements (eliminating double counting in cases where two filaments are mutually each other’s nearest neighbor). We ignore effects of an inclination angle  $i$  in this analysis, which could mean that the measured distances are less than the actual distances by a factor  $\sin i$ . Our measured filament spacings (which we equate with  $L_0$ ) have a minimum value 0.5 pc, a maximum value 2.2 pc, a median value 0.9 pc, and a mean value 1.0 pc.

#### 2.3.2. Estimate from star formation timescale

Another way to constrain  $L_0$  is through the star formation timescale in molecular clouds. Since this num-

ber is widely accepted to be in the range 1-3 Myr (Palla & Stahler 2000, 2002; Hartmann 2001), and star formation is often coordinated along a filament over this timescale, we can place an upper limit (again empirically) on the compression timescale  $t_0$  of a few Myr. Therefore the initial length scale that can trigger a compression can be written as

$$L_0 \simeq v_{t0} t_0 \simeq v_{A0} t_0, \quad (10)$$

where  $t_0$  is as above and again using the Alfvénic nature of turbulence. This further simplifies to

$$L_0 \simeq \frac{B_0}{\sqrt{4\pi\rho_0}} t_0 = \frac{\sqrt{2}}{\mu_0} c_s t_0, \quad (11)$$

where we have used pressure balance along the magnetic field,  $\pi G \Sigma_0^2 / 2 = \rho_0 c_s^2$  and the normalized mass-to-flux ratio  $\mu_0 = \Sigma_0 (2\pi\sqrt{G}) / B_0$ . If we consider the initial cloud to be mildly subcritical, i.e.,  $\mu_0 \approx 0.5$ , and a sound speed  $c_s = 0.2 \text{ km s}^{-1} \simeq 0.2 \text{ pc Myr}^{-1}$ , then  $t_0 \simeq 1 - 3 \text{ Myr}$  leads to  $L_0 \simeq 1 \text{ pc}$ .

## 3. RESULTS

The simple arguments of the previous section show that the length scale at which the ribbon formation is initiated is of the order of a parsec. Our semi-analytic model then implies that the final width of the ribbon given by equation (9) is  $\sim 0.3 \text{ pc}$ . However, the shortest dimension is flattened along the direction of the magnetic field and has a thickness  $2H$  that *does* depend on the column density. Therefore, the observed shape will depend on the viewing angle. Below we calculate the observed width for a particular viewing angle and then calculate a synthetic plot of observed ribbon width versus observed column density for a collection of random viewing angles. Our objective is to gain insight into the form of the observed correlation, and how it compares with the standard Jeans length scaling and with the observational results presented by Arzoumanian et al. (2011). The value of  $L_0$  can be considered a free parameter and physically may vary from one cloud to another and have a distribution of values within a single cloud. While we do not advocate a specific individual value for  $L_0$ , we use the empirical estimate that it should be  $\sim 1 \text{ pc}$  to determine the shape and approximate quantitative values of an observed correlation.

### 3.1. Observed Width

Let the normal to the filament, along the  $z$ -axis, be inclined at an angle  $\theta$  to the observer as shown in Fig. 2. For a ribbon-like filament of intrinsic width  $L$  and half thickness  $H$  the projected width  $L_{\text{obs}}$  as seen by the observer is

$$L_{\text{obs}} = L \cos \theta + 2H \sin \theta. \quad (12)$$

If the ribbon is viewed face on, i.e.,  $\theta = 0^\circ$ , the observed width is just the intrinsic width  $L$ . When viewed side on i.e.,  $\theta = 90^\circ$  the observed width is the thickness  $2H$  of the ribbon along the  $z$  axis. For any other intermediate angles one sees the projection in the  $y$ - $z$  plane i.e., equation (12), as shown in Fig. 2.

From our analysis we have already shown in equation (9) that the intrinsic width  $L$  is a fraction of the initial compression length scale  $L_0$ .

The thickness  $2H$  of the magnetic ribbon is evaluated using the hydrostatic equilibrium, equation (2), along the direction of the magnetic field (i.e., perpendicular to the filament width). For column density  $\Sigma = 2\rho H$ , the half-thickness of the clouds is estimated to be

$$H = \frac{c_s^2}{\pi G \Sigma}. \quad (13)$$

For a ribbon of any particular column density  $\Sigma$  we can estimate the corresponding half-thickness  $H$ , which is essentially the Jeans scale, using equation (13). For example,  $H = 0.16$  pc for  $c_s = 0.2 \text{ km s}^{-1}$  and  $N \equiv \Sigma/m = 10^{21} \text{ cm}^{-2}$  in which  $m = 2.3 m_H$ .

### 3.2. Observed Column Density

The observed column density  $\Sigma_{\text{obs}}$  will be different from the intrinsic column density  $\Sigma$  depending on the angle at which the ribbon is being viewed. If the observer is situated at angle other than  $\theta = \phi = 0^\circ$  (as shown in Fig. 2.2), the length along the line of sight changes thus affecting the observed column density. In the following section we will analyze the variation of  $\Sigma_{\text{obs}}$  with the viewing angles  $\theta$  and  $\phi$ . We neglect the variation of  $\rho$  within the ribbon.

#### 3.2.1. Case 1 ( $0^\circ \leq \theta \leq \theta_{\text{crit}}$ )

For the beam incident on the face of the ribbon at an angle  $0^\circ \leq \theta \leq \theta_{\text{crit}}$  and  $\phi = 0^\circ$ , (refer to Fig. 2a,) the observed column density is

$$\Sigma_{\text{obs}} = 2\rho H \sec \theta. \quad (14)$$

Since the intrinsic column density  $\Sigma = 2\rho H$ , we get

$$\Sigma_{\text{obs}} = \Sigma \sec \theta. \quad (15)$$

Thus only for  $\theta = 0^\circ$ , i.e., when the ribbon is viewed face on,  $\Sigma_{\text{obs}} = \Sigma$ . For  $0^\circ < \theta \leq \theta_{\text{crit}}$ ,  $\Sigma_{\text{obs}} > \Sigma$ .

#### 3.2.2. Case 2 ( $\theta = \theta_{\text{crit}}$ )

For the beam entering at a critical angle  $\theta_{\text{crit}}$  and  $\phi = 0^\circ$  (Fig. 2b), the observed column density is

$$\Sigma_{\text{obs}} = 2\rho H \sec \theta_{\text{crit}} = \rho L \csc \theta_{\text{crit}}. \quad (16)$$

Rearranging the above equation, we find that

$$\theta_{\text{crit}} = \tan^{-1} \frac{L}{2H}. \quad (17)$$

The critical angle  $\theta_{\text{crit}}$  separates the two sets of angles that have separate expressions for  $\Sigma_{\text{obs}}$ .

#### 3.2.3. Case 3 ( $\theta_{\text{crit}} \leq \theta \leq 90^\circ$ )

For the beam entering through the shorter dimension of the ribbon (see Fig. 2c) at an angle  $\theta_{\text{crit}} \leq \theta \leq 90^\circ$  and  $\phi = 0^\circ$ , the observed column density is

$$\Sigma_{\text{obs}} = \rho L \csc \theta. \quad (18)$$

Using equation (2), and  $\Sigma = 2\rho H$ , we get

$$\Sigma_{\text{obs}} = \frac{\Sigma L}{2H \sin \theta} = \frac{\pi G \Sigma^2 L}{2c_s^2 \sin \theta}. \quad (19)$$

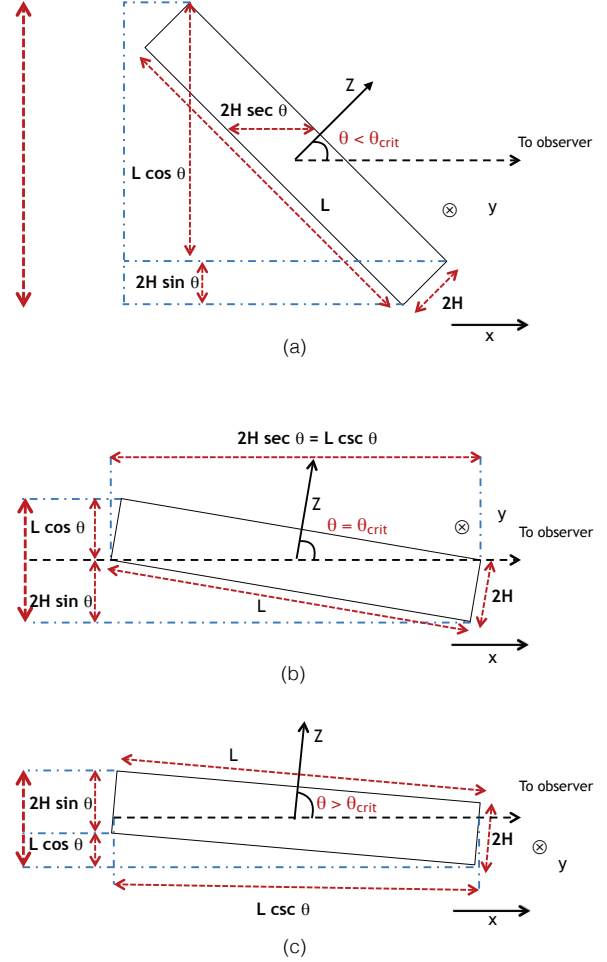


**Figure 2.** Different orientations of the magnetic ribbon with respect to the observer. Top panel: case 1 ( $0^\circ \leq \theta \leq \theta_{\text{crit}}$ ). Middle panel: case 2 ( $\theta = \theta_{\text{crit}}$ ) when the ribbon is observed at a critical angle as shown. Bottom panel: case 3 ( $\theta_{\text{crit}} \leq \theta \leq 90^\circ$ ).

For  $\theta = 90^\circ$ , i.e., when the ribbon is viewed side on,  $\Sigma_{\text{obs}} = \Sigma \frac{L}{2H}$ . For  $\theta_{\text{crit}} < \theta \leq 90^\circ$ ,  $\Sigma_{\text{obs}} > \Sigma$  if  $L > 2H$ , i.e., when the ribbon width is greater than the thickness of the ribbon, the observed column density is greater than the actual column density.

#### 3.2.4. Case 4 ( $\phi \neq 0^\circ$ )

Furthermore, different angular orientation of the magnetic ribbons in the  $x$ - $y$  plane will also alter the observed column density. If the long axis ( $y$ ) of the ribbon is not perpendicular the line of sight (see Fig. 2.2), i.e.,  $\phi \neq 0^\circ$  the observed column density will further increase. For any random orientation in the  $x$ - $y$  plane, the modified column density is

$$\Sigma_{\text{obs}} = \Sigma \sec \theta \sec \phi, \quad 0^\circ \leq \theta \leq \theta_{\text{crit}}, \quad (20)$$

$$\Sigma_{\text{obs}} = \frac{\pi G \Sigma^2 L}{2c_s^2 \sin \theta} \sec \phi, \quad \theta_{\text{crit}} \leq \theta \leq 90^\circ. \quad (21)$$

However, different orientations in the  $x$ - $y$  plane do not affect the observed ribbon width. The resultant projection of the ribbon width on the  $y$ - $z$  plane is independent of the azimuthal angle  $\phi$ .

### 3.3. Observed Correlation

Since the observations of Arzoumanian et al. (2011) reveal a relatively flat relation between observed width and column density, it is instructive to use our model to make a synthetic map of these quantities. For simplicity we consider  $\phi = 0$  in this analysis. We take a sample of 100 ribbons with number column density distributed uniformly in the range  $10^{21} \text{ cm}^{-2} \leq N \leq 10^{23} \text{ cm}^{-2}$ . Furthermore we take viewing angles randomly chosen in the range  $0^\circ \leq \theta \leq 90^\circ$ . Each pair of values  $(N, \theta)$  yields a pair of values  $(N_{\text{obs}}, L_{\text{obs}})$  represented as blue dots in Fig. 3. We obtain  $L_{\text{obs}}$  using equation (12) and  $\Sigma_{\text{obs}}$  using equation (15) or equation (19) for  $\theta \leq \theta_{\text{crit}}$  or  $\theta > \theta_{\text{crit}}$ , respectively. The black dashed line in Fig. 3 is the locus of points obtained by taking 100 randomly chosen values of  $\theta$  for each value of  $N$  and calculating the mean values of  $L_{\text{obs}}$  and  $N_{\text{obs}}$ . This line is similar to the result of taking equation (12) and inserting the mean values of  $\cos \theta$  and  $\sin \theta$ , which are both equal to  $2/\pi$ , and replacing  $\Sigma$  with the mean value of  $\Sigma_{\text{obs}}$ . However, the mean value of  $\Sigma_{\text{obs}}$  across all angles is not exactly equal to  $\Sigma$ . Both the set of individual synthetic data points shown in blue dots as well as the average relation in the black dashed line show a relatively flat relation over two orders of magnitude variation in  $N_{\text{obs}}$ . Fig. 3 also shows the analytic relation for two limiting cases. The black dotted line corresponds to the face on view ( $\theta = 0^\circ$ ) where  $L_{\text{obs}} = L = 0.3 \text{ pc}$  and is independent of the column density. The blue dot-dashed line corresponds to  $\theta = 90^\circ$  where  $L_{\text{obs}} = 2c_s^2/(\pi G \Sigma)$ , essentially the Jeans length.

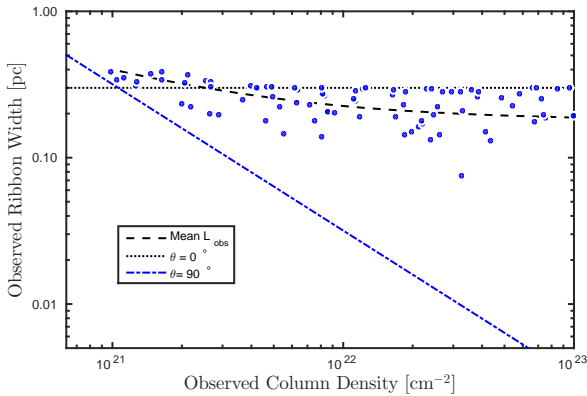


**Figure 3.** Apparent ribbon width  $L_{\text{obs}}$  versus observed column density  $N_{\text{obs}}$ . Each blue dot corresponds to a magnetic ribbon with intrinsic column density  $N$  and observing angle  $\theta$ , chosen as described in Sec. 3.3. The black dashed line is the mean ribbon width for the entire range of values of  $N_{\text{obs}}$ . The black dotted line is the width when the ribbon is viewed at  $\theta = 0^\circ$ . The blue dot-dashed line is the width for the side on view i.e.,  $\theta = 90^\circ$ .

## 4. CONCLUSION

We have presented a minimum hypothesis model for the width of a filament in a molecular cloud in which magnetic fields and magnetohydrodynamic turbulence are initially dominant. A turbulent compression leads to a magnetic ribbon whose thickness is set by the stand-off between ram pressure and magnetic pressure region. Gravitationally-driven ambipolar diffusion then leads to

runaway collapse of the densest regions in the ribbon, where the mass-to-flux ratio has become supercritical. This process has been demonstrated in published simulations of trans-Alfvénic turbulence in a cloud with an initial subcritical mass-to-flux ratio (e.g., Nakamura & Li 2005; Kudoh & Basu 2011). We have extended the semi-analytic model of Kudoh & Basu (2014) to estimate their lateral (perpendicular to magnetic field and ribbon long axis) width. This quantity is independent of the density of the ribbon. This lateral width can also be used to estimate the parent filament radius  $R_0$  in the theoretical magnetic ribbon model of Tomisaka (2014). In our model, the thickness parallel to the magnetic field is essentially the Jeans scale and does depend on density. Hence, we calculate a distribution of apparent widths seen in projection assuming a random set of viewing angles. The resulting distribution of apparent widths versus apparent column density is relatively flat (unlike expectations based on the Jeans length) over the range  $10^{21} \text{ cm}^{-2} - 10^{23} \text{ cm}^{-2}$ , in rough agreement with the observations of Arzoumanian et al. (2011). Other models have been introduced to explain the apparent near-uniform width of observed filaments. Fischera & Martin (2012) introduce an external pressure to an isothermal cylinder and find that the FWHM versus column density is a peaked function and approximately flat in the regime where  $m_l$  is well below  $m_{l,\text{crit}}$  and the external pressure is comparable to the central pressure. However, filaments with  $m_l > m_{l,\text{crit}}$  would be in a time-dependent state of dynamical collapse. Hennebelle & André (2013) develop a model of a cylindrical self-gravitating filament that is accreting at a prescribed rate. A near-uniform radius is derived based on assumption of a steady-state balance between energy input from accretion and dissipation of energy by ion-neutral friction at the filament radius scale. Heitsch (2013) also develops a model of accretion at the free-fall rate onto a filament with  $m_l < m_{l,\text{crit}}$  and uses various prescribed forms of internal structure to find that the FWHM has a peaked dependence on column density. A series of simulation papers (Smith et al. 2014; Kirk et al. 2015; Federrath 2016) use hydrodynamic or MHD simulations (with supercritical mass-to-flux ratio) and analyze filament widths at particular snapshots in time. Although their filament widths cluster at  $\sim 0.1 \text{ pc}$  with some scatter, there is a mild to strong density dependence of the widths, and the filaments are single time snapshots in a situation of continuing collapse. Federrath (2016) suggests that  $\sim 0.1 \text{ pc}$  is special since the linewidth-size relation of Larson (1981) would lead to subsonic turbulence below that scale, but it is not clear if his simulations satisfy this scaling internally. We believe that the magnetic ribbon model provides an alternative simplified interpretation that accounts for turbulence and strong magnetic fields. We have developed a method to estimate the width of a magnetic ribbon based on the characteristic scale and amplitude of MHD turbulence. Such ribbons can have a line mass that exceeds the hydrodynamic limit  $2c_s^2/G$  and still be in a dynamically oscillating quasi-equilibrium state. However, gravity still leads to star formation in the dense interior through rapid ambipolar diffusion.

We thank the anonymous referee for comments that

improved the discussion in this paper. This work was supported by a Discovery Grant from NSERC.

#### REFERENCES

- André, P., Men'shchikov, A., Bontemps, S., et al. 2010, *A&A*, 518, L102
- Arzoumanian, D., André, P., Didelon, P., et al. 2011, *A&A*, 529, L6
- Basu, S. 2000, *ApJ*, 540, L103
- Basu, S., Ciolek, G. E., Dapp, W. B., & Wurster, J. 2009, *NewA*, 14, 483
- Crutcher, R. M. 1999, *ApJ*, 520, 706
- Dapp, W. B., & Basu, S. 2009, *MNRAS*, 395, 1092
- Federrath, C. 2016, *MNRAS*, 457, 375
- Fiedler, R. A., & Mouschovias, T. C. 1993, *ApJ*, 415, 680
- Fischera, J., & Martin, P. G. 2012, *A&A*, 542, A77
- Hanawa, T., & Tomisaka, K. 2015, *ApJ*, 801, 11
- Hartmann, L. 2001, *AJ*, 121, 1030
- Heitsch, F. 2013, *ApJ*, 769, 115
- Hennnebelle, P., & André, P. 2013, *A&A*, 560, A68
- Kim, C.-G., & Basu, S. 2013, *ApJ*, 778, 88
- Kirk, H., Klassen, M., Pudritz, R., & Pillsworth, S. 2015, *ApJ*, 802, 75
- Kudoh, T., & Basu, S. 2008, *ApJ*, 679, L97
- . 2011, *ApJ*, 728, 123
- . 2014, *ApJ*, 794, 127
- Larson, R. B. 1981, *MNRAS*, 194, 809
- . 1985, *MNRAS*, 214, 379
- Li, Z.-Y., & Nakamura, F. 2004, *ApJ*, 609, L83
- Men'shchikov, A., André, P., Didelon, P., et al. 2010, *A&A*, 518, L103
- Mouschovias, T. C., & Spitzer, Jr., L. 1976, *ApJ*, 210, 326
- Nakamura, F., & Li, Z.-Y. 2005, *ApJ*, 631, 411
- . 2008, *ApJ*, 687, 354
- Ostriker, J. 1964, *ApJ*, 140, 1056
- Palla, F., & Stahler, S. W. 2000, *ApJ*, 540, 255
- . 2002, *ApJ*, 581, 1194
- Palmeirim, P., André, P., Kirk, J., et al. 2013, *A&A*, 550, A38
- Panopoulou, G. V., Tassis, K., Goldsmith, P. F., & Heyer, M. H. 2014, *MNRAS*, 444, 2507
- Planck Collaboration, Ade, P. A. R., Aghanim, N., et al. 2016, *A&A*, 586, A138
- Schneider, S., & Elmegreen, B. G. 1979, *ApJS*, 41, 87
- Smith, R. J., Glover, S. C. O., & Klessen, R. S. 2014, *MNRAS*, 445, 2900
- Spitzer, Jr., L. 1942, *ApJ*, 95, 329
- Tomisaka, K. 2014, *ApJ*, 785, 24